JCTC Journal of Chemical Theory and Computation

Study of Proton Coupled Electron Transfer in a Biomimetic Dimanganese Water Oxidation Catalyst with Terminal Water Ligands

Ting Wang, Gary W. Brudvig, and Victor S. Batista*

Department of Chemistry, Yale University, P.O. Box 208107, New Haven, Connecticut 06520-8107

Received May 19, 2010

Abstract: The oxomanganese complex $[H_2O(terpy)Mn^{III}(\mu\text{-}O)_2Mn^{IV}(terpy)H_2O]^{3+}$ (**1**, terpy = 2,2′:6-2″-terpyridine) is a biomimetic model of the oxygen-evolving complex of photosystem II with terminal water ligands. When bound to TiO_2 surfaces, **1** is activated by primary oxidants (e.g., Ce^{4+}(aq) or oxone in acetate buffers) to catalyze the oxidation of water yielding O_2 evolution [G. Li et al. *Energy Environ. Sci.* **2009**, *2*, 230−238]. The activation is thought to involve oxidation of the inorganic core $[Mn^{III}(\mu\text{-}O)_2Mn^{IV}]^{3+}$ to generate the $[Mn^{IV}(\mu\text{-}O)_2Mn^{IV}]^{4+}$ state $\mathbf{1}_{ox}$ first and then the highly reactive Mn oxyl species $Mn^{IV}O^{\bullet}$ through proton coupled electron transfer (PCET). Here, we investigate the step **1** → $\mathbf{1}_{ox}$ as compared to the analogous conversion in an oxomanganese complex without terminal water ligands, the $[(bpy)_2\ Mn^{III}(\mu\text{-}O)_2\ Mn^{IV}\ (bpy)_2]^{3+}$ complex (**2**, bpy = 2,2′-bipyridyl). We characterize the oxidation in terms of free energy calculations of redox potentials and pK_a's as directly compared to cyclic voltammogram measurements. We find that the pK_a's of terminal water ligands depend strongly on the oxidation states of the Mn centers, changing by ∼13 pH units (i.e., from 14 to 1) during the III,IV → IV,IV transition. Furthermore, we find that the oxidation potential of **1** is strongly dependent on pH (in contrast to the pH-independent redox potential of **2**) as well as by coordination of Lewis base moieties (e.g., carboxylate groups) that competitively bind to Mn by exchange with terminal water ligands. The reported analysis of ligand binding free energies, pK_a's, and redox potentials indicates that the III,IV → IV,IV oxidation of **1** in the presence of acetate (AcO^-) involves the following PCET: $[H_2O(terpy)Mn^{III}(\mu\text{-}O)_2Mn^{IV}(terpy)AcO]^{2+} \rightarrow [HO(terpy)Mn^{IV}(\mu\text{-}O)_2Mn^{IV}(terpy)AcO]^{2+} + H^+ + e^-$.

I. Introduction

Studies of redox transitions in synthetic oxomanganese compounds can provide fundamental insights on analogous redox processes in the oxygen-evolving complex (OEC) of photosystem II (PSII),[1−7] and in artificial photosynthetic systems based on biomimetic complexes.[8−10] The main challenge is to gain understanding of 'redox-leveling' processes where proton coupled electron transfer (PCET) leads to the accumulation of multiple oxidizing equivalents over a low range of potential. This paper explores the PCET mechanism associated with the oxidation of the oxomanganese complex $[H_2O(terpy)Mn^{III}(\mu\text{-}O)_2Mn^{IV}(terpy)H_2O]^{3+}$ (**1**, terpy = 2,2′:6-2″-terpyridine), shown in Figure 1, forming

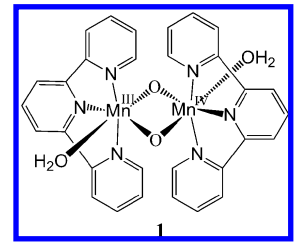

Figure 1. Schematic of complex **1** $[(H_2O)(terpy)Mn^{III}(\mu\text{-}O)_2Mn^{IV}(terpy)(H_2O)]^{3+}$ (terpy = 2,2′:6-2″-terpyridine).

* Corresponding author. Fax: +1 203 432 6144, E-mail: victor.batista@yale.edu.

10.1021/ct1002658
Published on Web 07/15/2010

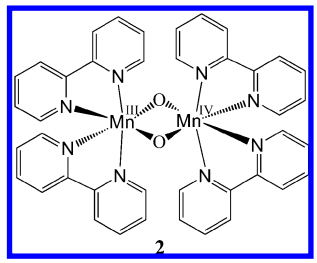

Figure 2. Schematic of complex **2** $[(bpy)_2Mn^{III}(\mu\text{-}O)_2Mn^{IV}\text{-}(bpy)_2]^{3+}$ (bpy = 2,2′ bipyridyl).

the $\mathbf{1}_{ox}$ state through the oxidation $[Mn^{III}(\mu\text{-}O)_2Mn^{IV}]^{3+} \rightarrow [Mn^{IV}(\mu\text{-}O)_2Mn^{IV}]^{4+}$ of its inorganic core.[8,11−18]

Several Mn complexes have been proposed as structural models of the OEC of PSII where Mn ions are connected by μ-oxo linkages (i.e., deprotonated water molecules).[17,19−34] In addition to complex **1**, other Mn dimers were studied,[25,27,28] including the mixed valence Mn dimer **2** $[(bpy)_2\ Mn^{III}\ (\mu\text{-}O)_2\ Mn^{IV}\ (bpy)_2]^{3+}$ (bpy = 2,2′- bipyridyl), shown in Figure 2 (originally synthesized by Nyholm and Turco[29] and characterized by X-ray diffraction spectroscopy by Plaksin et al)[30] as well as Mn trimers[26] and tetramers.[22,31−34] Oxygen evolution catalyzed by complex **1** has been the subject of several studies.[8,11−16] However, the underlying catalytic mechanism and the nature of the reaction intermediates remain only partially understood.[12,14] It is, therefore, essential to advance our understanding of the reaction pathways, including changes in the protonation states of the ligands and the influence of competitive ligands that affect the redox potentials when binding to Mn.

The computations reported in this paper aim to provide a thorough characterization of the $\mathbf{1} \rightarrow \mathbf{1}_{ox}$ redox state transition, complementing earlier studies on the capabilities of density functional theory (DFT) methods for predictions of redox potentials of transition-metal complexes.[17,35−52] Most of these previous studies investigated functionals based on the generalized gradient approximation (GGA), such as BLYP,[53] BP86,[54] and Perdew−Burke−Ernzerhof (PBE)[55] as well as hybrid functionals (e.g., B3LYP),[56,57] including studies of oxomanganese complexes.[17,58] However, the analysis of PCET mechanisms in biomimetic oxomanganese complexes with terminal water ligands has yet to be reported and is addressed in this paper, including the regulatory effect of carboxylate binding on the redox properties of the complex.

In a recent study, we have shown that **1** binds to TiO_2 nanoparticles (NPs) by direct deposition, exchanging a water ligand by the TiO_2 NP.[8] Attachment to NPs with different degrees of crystallinity, including Degussa P25 (∼85% anatase and ∼15% rutile) and synthetic TiO_2 (sintered at 450 °C, D450, or without thermal treatment D70) was characterized by electron paramagnetic resonance (EPR), UV−vis spectroscopy, and electrochemistry. In addition, O_2 evolution was observed upon activation of **1** deposited on P25 using Ce^{4+} (or oxone in acetate buffer) as a primary oxidant.[8] However, understanding the underlying oxidation process still requires clarification of the nature of the ligation scheme, including the exchange of water by acetate ligands or TiO_2 NP's as well as changes in the protonation states of terminal waters and oxo/hydroxo bridges.

Cyclic voltammograms of **1** deposited on TiO_2 surfaces indicated that the redox activity of **1** was similar to its behavior in solution,[8,12,18,59] including a quasi-reversible redox couple at ∼1 V (P_a^1 and P_c^1)[8] assigned to the $\mathbf{1} \leftrightarrow \mathbf{1}_{ox}$ conversion and a broad cathodic wave at ca. 850 mV (P_c^2) due to reduction of the Mn^{IV} tetramer formed by spontaneous dimerization of $\mathbf{1}_{ox}$. In this study, we focus on the pH dependence of the redox potential associated with the $\mathbf{1} \leftrightarrow \mathbf{1}_{ox}$ conversion. In addition, we analyze the effect of oxidation on the pK_a's of terminal waters and acetate binding to Mn. The results are compared to the analogous (III,IV) → (IV,IV) transition in complex **2** where there are no water ligands involved. The reported analysis builds upon our recent work on the characterization of the oxidation state transition (III,III) → (III,IV) in **2**, as analyzed according to DFT calculations of redox potentials and pK_a's obtained by using the standard thermodynamic cycle formalism applied in conjunction with continuum solvation models.[58] The computational results provided fundamental insight on the mechanism responsible for the pH dependence of redox potentials, as described by the Pourbaix diagrams reported by voltammogram measurements,[25] where the linear dependence of $E_{1/2}$ with pH in the range pH = 3−9 (with a ∼59 mV/pH slope) was consistent with the one-electron one-proton couple $[(bpy)_2Mn^{III}(\mu\text{-}O)_2Mn^{IV}(bpy)_2]^{3+} + H^+ + e^- \rightarrow [(bpy)_2Mn^{III}(\mu\text{-}O)(\mu{-}OH)\text{-}Mn^{III}(bpy)_2]^{3+}$.[58] The agreement between theory and experiments showed that the DFT B3LYP level provided accurate descriptions of the regulatory effect of oxidations on the pK_a's of μ-hydroxo ligands as well as the effect of deprotonation of the bridges on the redox potentials of the metal centers. Here, we extend these earlier studies to explore the role of terminal water ligands in the regulation of redox potentials of complex **1**, including the analysis of deprotonation and carboxylate binding on the $\mathbf{1} \leftrightarrow \mathbf{1}_{ox}$ oxidation state transition. The reported analysis of PCET, coupling oxidation state transitions of Mn and deprotonation of water ligands attached to those metal centers, should provide insights on redox-leveling processes in the OEC of PSII[1−7] and artificial photosynthetic systems.[11,14,60]

The paper is organized as follows. Section II outlines the computational methods applied for calculations of pK_a's and redox potentials. Section III presents our computational results and direct comparisons with experimental measurements. Concluding remarks and future research directions are outlined in Section IV.

II. Computational Methods

The methods implemented in this study have already been described in our previous work on oxomanganese complexes.[17,58] Here, we outline the computational methodology only briefly.

Electronic Structure Calculations. All electronic structures were obtained at the Becke-3−Lee−Yang−Parr (B3LYP) DFT level,[56,57] using the Jaguar suite of electronic structure programs. Minimum energy configurations of complexes **1** and **2** in the reduced (III,IV) and oxidized (IV,IV) states were obtained in broken symmetry (BS) spin

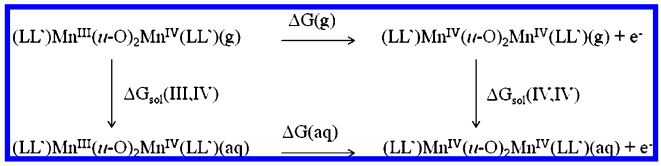

Figure 3. Born−Haber thermodynamic cycle used for calculations of free energy changes $\Delta G(\text{aq}) = -nFE^0$ yielding the standard redox potentials E^0, as described in the text, with L = terpy and L′ = H_2O for complex **1** and L = L′ = bpy for complex **2**.

states with α and β electronic densities localized on different metal centers.[61,62] All optimizations involved unrestricted Kohn−Sham wave functions (UB3LYP) and yielded antiferromagnetically coupled high-spin manganese centers. We applied a mixed basis set, including the LACVP basis that accounts for a nonrelativistic description of effective core potentials (ECPs) for the Mn^{4+} and Mn^{3+} centers, the 6-31G (2df) basis sets including polarization functions for μ-oxo O^{2-} species, and the 6-31G basis sets for the rest of the atoms. All optimizations were followed by UB3LYP single point energy calculations based on Dunning's correlation-consistent triple-ζ basis set[63−65] cc-pVTZ(-f), including a double set of polarization functions. Very similar results were also obtained for the cc-pVTZ(-f)++ basis set, as previously reported for other systems.[43]

Calculations of Standard Potentials. The half-cell standard potentials E^0 for the redox state transitions (III,IV) ↔ (IV,IV) of complexes **1** and **2** were obtained from DFT calculations of free energy changes $\Delta G(\text{aq}) = -nFE^0$, where $n = 1$ is the number of electrons involved in the redox couple and $F = 23.06$ kcal mol^{-1} V^{-1} is the Faraday constant. Redox potentials were reported relative to the normal hydrogen electrode (NHE), experimentally determined to be 4.43 eV.[66] Therefore, we have subtracted 4.43 V from the absolute potentials to make direct comparisons to cyclic voltammogram data referred to the NHE.

Free Energy Calculations of Standard Potentials. Using the Born−Haber cycle, depicted in Figure 3, we computed $\Delta G(\text{aq}) = \Delta G(\text{g}) + \Delta G_{\text{sol}}(\text{III,III}) - \Delta G_{\text{sol}}(\text{III,IV})$ from the free energy change $\Delta G(\text{g}) = \Delta H(\text{g}) - T\Delta S(\text{g})$ due to the redox state transition in the gas phase, where $\Delta H(\text{g}) = \Delta H_{\text{EA}}(\text{DFT}) + \Delta H_{\text{ZPE}} + \Delta H_{\text{T}}$ was obtained from the DFT electron attachment enthalpies $\Delta H_{\text{EA}}(\text{DFT})$ in the gas phase, while the changes in the zero point energy ΔH_{ZPE} and the corrections for molecular entropy changes $\Delta S(\text{g})$ were based on vibrational frequency calculations.

The solvation free energies $\Delta G_{\text{sol}}(\text{III,IV})$ and $\Delta G_{\text{sol}}(\text{IV,IV})$ were computed by using the self-consistent reaction field (SCRF) approach of standard continuum solvation models.[67,68] All calculations were based on gas-phase geometries employing the dielectric constant of water ($\varepsilon = 80.37$) for the continuum medium and on a solvent radius of 1.40 Å. Corrections due to hydrogen bonding with solvent molecules and changes in the thermal enthalpy ΔH_{T} were neglected.[43]

Free Energy Calculations of pK_a's. The pK_a's of water terminal ligands were obtained by computing the DFT free energy changes $\Delta G_a(\text{aq})$ due to deprotonation of the complexes, as follows: $\text{p}K_a = \beta\Delta G_a(\text{aq})$, where $\beta = (k_B T)^{-1}$ with

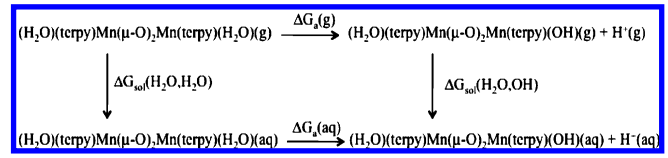

Figure 4. Born−Haber thermodynamic cycle used for calculations of free energy changes $\Delta G_a(\text{aq}) = k_B T\,\text{p}K_a$ yielding the pK_a of terminal water ligands in complex **1**.

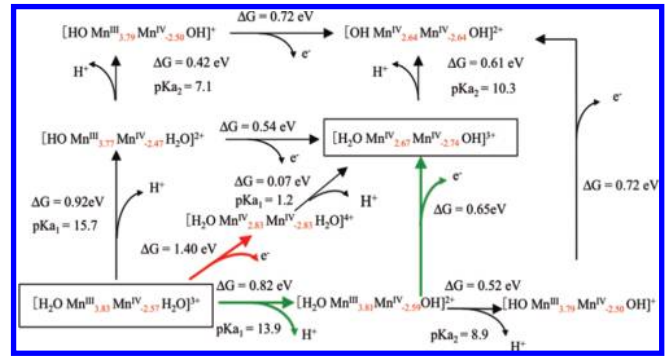

Figure 5. Thermodynamic diagram of PCET for complex **1** in aqueous solutions at pH = 0, obtained from free energy calculations of redox potentials and pK_a's at the DFT B3LYP/cc-pVTZ(-f) level, based on the Haber-Born cycle method applied in conjunction with a continuum solvation model. Formal oxidation numbers are indicated as superscripts in roman numbers, and the spin populations obtained according to the Mulliken population analysis are indicated as subscripts in red. For simplicity, the terpyridine ligands attached to Mn centers have been omitted.

$T = 298.15$ K, and k_B is the Boltzmann constant. The values of $\Delta G_a(\text{aq})$, due to deprotonation of the terminal water ligands for complex **1** in aqueous solutions, were obtained by using the Born−Haber cycle depicted in Figure 4, as follows:

$$\Delta G_a(\text{aq}) = \Delta G_a(\text{g}) + \Delta G_{\text{sol}}(\text{H}_2\text{O,OH}) + \Delta G_{\text{sol}}(\text{H}^+) - \Delta G_{\text{sol}}(\text{H}_2\text{O,H}_2\text{O}) \quad (5)$$

where $\Delta G_a(\text{g}) = \Delta H_a(\text{g}) - T\Delta S_a(\text{g})$ is the free energy change due to deprotonation of **1** in the gas phase, and $\Delta H_a(\text{g}) = \Delta H_a(\text{DFT}) + \Delta H_{\text{ZPE}} + \Delta H_{\text{T}}$ is the total enthalpy change obtained from the DFT energy change $\Delta H_a(\text{DFT})$. The solvation free energies associated with the protonated and deprotonated forms of the complex, $\Delta G_{\text{sol}}(\text{H}_2\text{O,H}_2\text{O})$ and $\Delta G_{\text{sol}}(\text{H}_2\text{O,OH})$, respectively, were estimated by using continuum solvation models, with the solvation free energy of H^+ in water $\Delta G_{\text{sol}}(\text{H}^+)$ taken as −260 kcal mol^{-1}.[66,69,70]

III. Results

Figure 5 shows the free energy diagram for PCET in complex **1** obtained, as described in Section II, from calculations of redox potentials and pK_a's at the DFT B3LYP/cc-pVTZ(-f) level of theory. The diagram shows that the (III,IV) state of complex **1** has terminal water ligands at pH < 13.9, while the oxidized (IV,IV) state spontaneously deprotonates one of its water ligands at pH > 1.2. In addition, the results summarized in Figure 5 show that the (III,IV) → (IV,IV) oxidation of **1** requires only 0.65

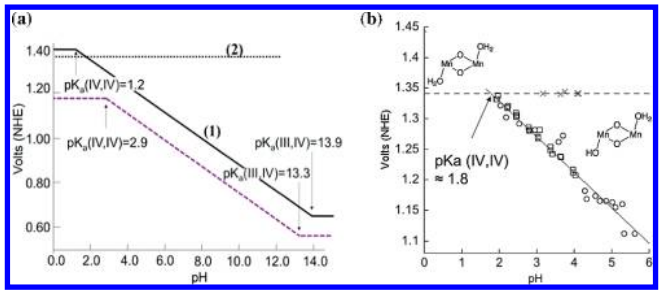

Figure 6. (a) Pourbaix diagrams for complexes **1** and **2**, obtained from free energy calculations of redox potentials and pK_a's at the DFT B3LYP/cc-pVTZ(-f) level of theory, in aqueous solutions (black solid line) and with acetate binding (purple dashed line). (b) Experimental CV data (open circles, ○, and squares, □, for **1** and crosses, ×, for **2**), as reported in ref 18.

V at pH > 13.9 after the water ligand bound to Mn^{IV} is deprotonated forming $[H_2O(terpy)Mn^{III}(\mu\text{-}O)_2Mn^{IV}terpy)\text{-}(OH]^{2+}$, while oxidation before deprotonation (at pH < 1.2) is thermodynamically much more demanding ($E^0 = 1.40$ V).

For intermediate values of pH = 1.2−13.9, the oxidation is coupled to deprotonation through PCET. The total energy requirement for the (III,IV) → (IV,IV) oxidation of **1** includes (0.82−0.059 pH) eV to deprotonate the water ligand bound to Mn^{IV}, plus 0.65 eV necessary to oxidize Mn^{III} in the deprotonated complex $[H_2O(terpy)Mn^{III}(\mu\text{-}O)_2Mn^{IV}\text{-}(terpy)OH]^{2+}$. Therefore, by coupling the deprotonation and the oxidation by PCET, the complex can be oxidized at a potential (0.65 + 0.82 − 0.059 pH) V lower than 1.4 V and deprotonated at pH < 13.9. In contrast, in the absence of coupling, the water ligand bound to Mn^{IV} deprotonates only at pH ≥ 13.9, and the complex is oxidized only at voltage ≥1.4 V. In a cyclic voltammogram (CV) measurement, the deprotonation during PCET is driven by the externally applied electric field. Therefore, at pH = 1.2−13.9, the position of the CV peak accounts for both free energy changes, including the deprotonation of the water ligand and the oxidation of the Mn center, yielding a redox potential that changes linearly by 59 mV per pH unit.

Figure 6, left panel, shows the Pourbaix diagram based on ab initio calculations of pK_a's and redox potentials obtained at the DFT B3LYP/cc-pVTZ(-f) level of theory. These calculations predict the redox potential of **1** for the entire pH range, without relying on any kind of experimental data. The experimental CV measurements (Figure 6, right panel) were carried out as described in ref 18.

The calculations for **1** in aqueous solutions predict a linear dependence of $E_{1/2}$ with pH, changing at a rate of 59 mV/pH within the 1.2 < pH < 13.9 range (Figure 6, left panel) in agreement with experimental data (Figure 6, right panel).[18] Beyond this pH range (i.e., at either pH < 1.2 or pH > 13.9), the oxidation of **1** is pH-independent (non-PCET) with the crossover points of pH-independent and -dependent processes defined by the pK_a's of the water ligands in the (III,IV) and (IV,IV) oxidation states. In contrast to the pH-dependent results obtained for complex **1**, the calculated redox potential of **2** is constant ($E^0 = 1.36$ eV) and pH independent since the oxo bridges in **2** are deprotonated at pH > 2.[58] These

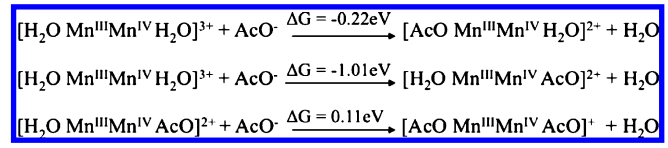

Figure 7. Free energy changes upon acetate (AcO^-) binding to complex **1**, obtained at the DFT B3LYP/cc-pVTZ(-f) level of theory. For simplicity, oxo bridges and terpy ligands attached to Mn centers have been omitted.

results are consistent with the CV data for **2** (Figure 6, right panel) which show a reversible one-electron anodic couple at $E_{1/2} = 1.34$ V (vs NHE), assigned to the oxidation of the III,IV complex to the IV,IV state[19,71] that is independent of pH. The favorable comparison between theory and experiments, shown in Figure 6, indicates that the DFT B3LYP/cc-pVTZ(-f) level of theory provides redox potentials for biomimetic oxomanganese complexes with terminal water molecules that agree with the experimental values within an estimated error of ±60 mV, yielding a semiquantitative description of PCET.

In order to investigate the regulatory effect of carboxylate moieties upon competitive binding to Mn by exchange with terminal ligands, we have analyzed the free energy changes due to exchange of water ligands of **1** by acetate. Figure 7 shows that either of the two water ligands (but not both) can spontaneously exchange with acetate, with binding to Mn^{IV} yielding the most stable complex in aqueous solution.

The calculations of binding affinities, shown in Figure 7, indicate that the predominant species in acetate buffers is $[H_2O(terpy)Mn^{III}(\mu\text{-}O)_2Mn^{IV}(terpy)AcO]^{2+}$. The Pourbaix diagram of such a complex, shown in Figure 6 (left panel, purple dashed line), indicates that the acetate binding stabilizes the oxidized form of the complex throughout the whole pH range, decreasing the redox potential of the III→IV transition by as much as 90−220 mV.

Figure 8 shows the detailed analysis of the effect of acetate on the underlying PCET mechanism in complex **1**, as characterized by calculations of redox potentials and pK_a's at the DFT B3LYP/cc-pVTZ(-f) level. It is shown that acetate binding changes the first pK_a of the water ligand from 13.9 to 13.3, in the Mn(III,IV) state and from 1.2 to 2.9 in the Mn(IV,IV) state. Consequently, the pH-range for PCET is shifted from pH = 1.2−13.9 in the absence of acetate to pH = 2.9−13.3 with acetate binding. In addition, Figure 8 shows that acetate binding to Mn^{IV} reduces the pH-independent oxidation potentials from 1.40 to 1.18 V at low pH when H_2O is bound to Mn^{III} and from 0.65 to 0.56 V at high pH when HO^- is ligated to Mn^{III}. Therefore, the redox potential of **1** is 1.18 V at pH < 2.9, since the oxidation takes the red pathway in Figure 8. At pH = 2.9−13.3, the potential decreases linearly at a rate of 59 mV/pH due to PCET (green path with nonspontaneous deprotonation), while at pH > 13.3 it remains constant at 0.56 V, since there is spontaneous deprotonation and the green path in Figure 8 prevails. The first crossover is defined by the pK_a of Mn(IV,IV), the pH at which the red and green pathways are energetically identical. Analogously, the pH of the subsequent crossover point is defined by the pK_a value of Mn(III,IV). The complete

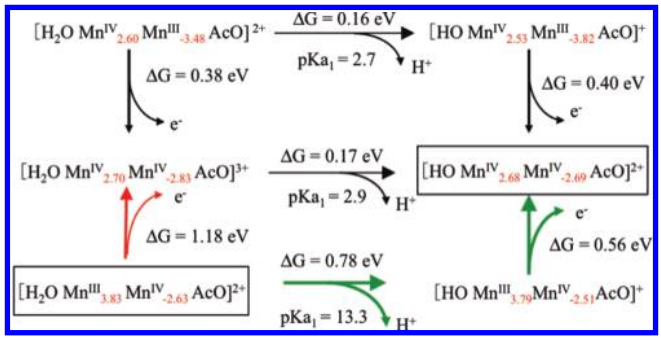

Figure 8. Thermodynamic diagram of PCET for complex **1** with acetate (AcO^-) binding in aqueous solutions at pH = 0, obtained from free energy calculations of redox potentials and pK_a's at the DFT B3LYP/cc-pVTZ(-f) level, based on the Born−Haber cycle method applied in conjunction with a continuum solvation model. Formal oxidation numbers are indicated as superscripts in roman numbers, and the spin populations obtained according to the Mulliken population analysis are indicated as subscripts in red. For simplicity, oxo bridges and terpy ligands attached to Mn centers have been omitted.

description provided by the reported binding energies, pK_a's, and redox potentials indicates that one of the two water ligands in **1** must exchange with acetate, yielding the III,IV → IV,IV oxidation state transition: $[H_2O(terpy)Mn^{III}(\mu\text{-}O)_2Mn^{IV}(terpy)AcO]^{2+} \rightarrow [HO(terpy)Mn^{IV}(\mu\text{-}O)_2Mn^{IV}(terpy)AcO]^{2+} + H^+ + e^-$, involving PCET in the pH = 2.9−13.3 range.

Our analysis of the oxidation mechanism of complex **1**, as influenced by the protonation states of water terminal ligands and the competitive binding of carboxylate moieties, suggests the following trends that might be common to other oxomanganese complexes: (1) at least one carboxylate moiety per high-valent di-μ-oxo-bridged Mn dimer can exchange with terminal water ligands and bind to Mn; (2) the redox potential of the di-μ-oxo-bridged Mn dimer is typically reduced by 100−200 mV upon carboxylate binding and by 620−750 mV upon deprotonation of a terminal water ligand; and (3) carboxylate binding reduces the pH range for PCET by about 2 pH units. Similar effects due to coordination of carboxylate moieties and deprotonation of water ligands might be expected in the OEC of PSII, where the regulatory mechanism based on PCET is thought to prevent the buildup of charge in the cluster through deprotonation of water/hydroxo ligands coupled to oxidation state transitions.

The molecular structure of the OEC of PSII remains only partially understood,[7] and several structural models have been proposed, including the '3 + 1 Mn tetramer'.[2,3] Such a model consists of a cuboidal structure of oxo-bridged high-valent Mn ions chelated by terminal water ligands as well as carboxylate and imidazole moieties from the surrounding protein amino acids. The model is partially consistent with mechanistic studies of water oxidation and high-resolution spectroscopy, although the structural and functional roles played by the ligands, including their potential "redox leveling" role during PCET, are yet to be established. The results reported for complex **1** suggest that ligation of carboxylate moieties and deprotonation of water ligands might be responsible for a similar redox leveling processes, leading to redox steps over a narrow range of potential during the accumulation of four oxidizing equivalents in the OEC.

IV. Conclusions

We have shown that the density functional theory (DFT) B3LYP/cc-pVTZ(-f) analysis of redox potentials and pK_a's of oxomanganese complexes with terminal water ligands provides a useful description of proton coupled electron transfer (PCET) at the detailed molecular level as well as a fundamental understanding of the regulatory effect of carboxylate moieties that bind competitively to Mn by exchange with terminal water ligands. The analysis provides understanding on the regulatory effect of oxidation state transitions on the pK_a's of terminal water ligands as well as the effect of deprotonation of water ligands, or exchange by carboxylate moieties, on the redox potentials of the Mn centers.

We conclude that PCET reduces the redox potential of **1** by coupling the deprotonation of the water ligand bound to Mn^{IV} to the oxidation of the Mn^{III} center, yielding oxidation at a potential (0.65 + 0.82 − 0.059 pH) V lower than the voltage 1.4 V required in the absence of deprotonation at pH < pK_a = 13.9. In the absence of such coupling, both of these processes are not favorable in the corresponding range of voltage and pH, since the water ligand deprotonates only at pH ≥ 13.9 and the complex is oxidized only at ≥1.4 V. We conclude that the exchange of water by acetate reduces the redox potential of the III,IV → IV,IV transition by 100−200 mV and the pH-range for PCET by about 2 pH units. Upon acetate binding to Mn^{IV}, PCET involves deprotonation of water ligated to Mn^{III} along the following oxidation state transition: $[H_2O(terpy)Mn^{III}(\mu\text{-}O)_2Mn^{IV}(terpy)AcO]^{2+} \rightarrow [HO(terpy)Mn^{IV}(\mu\text{-}O)_2Mn^{IV}(terpy)AcO]^{2+} + H^+ + e^-$. The resulting PCET mechanism thus prevents the accumulation of charge in the complex during the oxidation of the complex even at pH below the pK_a of the water ligand.

The observed regulatory effects, due to coordination of carboxylate moieties or deprotonation of water ligands, are expected to be common to PCET in other oxomanganese complexes, including the oxygen-evolving complex (OEC) of photosystem II (PSII) where deprotonation of water/hydroxo ligands is thought to be crucial to prevent charge buildup during the accumulation of multiple oxidation equivalents in the catalytic site. However, a direct simulation of PCET processes in the OEC of PSII is expected to be more challenging due to the presence of an inhomogeneous protein environment surrounding the metal complex, a problem that might require a combined quantum mechanics/molecular mechanics (QM/MM) method, as implemented in our previous studies of PSII.[1−7]

The predicted exchange of water by acetate in complex **1** suggests that other Lewis bases could readily exchange with terminal water ligands in oxomanganese complexes and reduce the redox potential of the complex, including buffer moieties commonly used in electrochemical measurements (e.g., phosphate), oxide groups on semiconductor nanoparticles surfaces (e.g., yielding direct deposition of the complex on the surface), or oxide ligands from other complexes that might yield oligomerization.

Acknowledgment. V. S. Batista acknowledges supercomputer time from NERSC and financial support from the grant NIH 1R01-GM-084267-01. G. W. Brudvig acknowledges support from the grant NIH GM32715.

Supporting Information Available: Description of the computational methods, nuclear coordinates, the spin population analysis, and the effect of oxidation state transition coupled to protonation/deprotonation events on the electrostatic potential atomic charges. Thermodynamic data, including solvation enthalpies and entropies are also provided. This information is available free of charge via the Internet at http://pubs.acs.org/.

References

(1) McEvoy, J. P.; Brudvig, G. W. *Chem. Rev.* **2006**, *106* (11), 4455–4483.

(2) Sproviero, E. M.; Gascon, J. A.; McEvoy, J. P.; Brudvig, G. W.; Batista, V. S. *J. Am. Chem. Soc.* **2008**, *130* (21), 6728–6730.

(3) Sproviero, E. M.; Gascon, J. A.; McEvoy, J. P.; Brudvig, G. W.; Batista, V. S. *J. Am. Chem. Soc.* **2008**, *130* (11), 3428–3442.

(4) Sproviero, E. M.; Gascon, J. A.; McEvoy, J. P.; Brudvig, G. W.; Batista, V. S. *J. Chem. Theory Comput.* **2006**, *2* (4), 1119–1134.

(5) Sproviero, E. M.; Gascon, J. A.; McEvoy, J. P.; Brudvig, G. W.; Batista, V. S. *Curr. Opin. Struct. Biol.* **2007**, *17* (2), 173–180.

(6) Ferreira, K. N.; Iverson, T. M.; Maghlaoui, K.; Barber, J.; Iwata, S. *Science* **2004**, *303* (5665), 1831–1838.

(7) Sproviero, E. M.; Gascon, J. A.; McEvoy, J. P.; Brudvig, G. W.; Batista, V. S. *Coord. Chem. Rev.* **2008**, *252* (3−4), 395–415.

(8) Li, G. H.; Sproviero, E. M.; Snoeberger, R. C.; Iguchi, N.; Blakemore, J. D.; Crabtree, R. H.; Brudvig, G. W.; Batista, V. S. *Energy Environ. Sci.* **2009**, *2* (2), 230–238.

(9) McNamara, W. R.; Snoeberger, R. C.; Li, G.; Schleicher, J. M.; Cady, C. W.; Poyatos, M.; Schmuttenmaer, C. A.; Crabtree, R. H.; Brudvig, G. W.; Batista, V. S. *J. Am. Chem. Soc.* **2008**, *130* (43), 14329–14338.

(10) Abuabara, S. G.; Cady, C. W.; Baxter, J. B.; Schmuttenmaer, C. A.; Crabtree, R. H.; Brudvig, G. W.; Batista, V. S. *J. Phys. Chem. C* **2007**, *111* (32), 11982–11990.

(11) Limburg, J.; Vrettos, J. S.; Liable-Sands, L. M.; Rheingold, A. L.; Crabtree, R. H.; Brudvig, G. W. *Science* **1999**, *283* (5407), 1524–1527.

(12) Baffert, C.; Romain, S.; Richardot, A.; Lepretre, J. C.; Lefebvre, B.; Deronzier, A.; Collomb, M. N. *J. Am. Chem. Soc.* **2005**, *127* (39), 13694–13704.

(13) Collomb, M. N.; Deronzier, A.; Richardot, A.; Pecaut, J. *New J. Chem.* **1999**, *23* (4), 351–353.

(14) Yagi, M.; Narita, K. *J. Am. Chem. Soc.* **2004**, *126* (26), 8084–8085.

(15) Chen, H. Y.; Tagore, R.; Olack, G.; Vrettos, J. S.; Weng, T. C.; Penner-Hahn, J.; Crabtree, R. H.; Brudvig, G. W. *Inorg. Chem.* **2007**, *46* (1), 34–43.

(16) Limburg, J.; Vrettos, J. S.; Chen, H. Y.; de Paula, J. C.; Crabtree, R. H.; Brudvig, G. W. *J. Am. Chem. Soc.* **2001**, *123* (3), 423–430.

(17) Sproviero, E. M.; Gascon, J. A.; McEvoy, J. P.; Brudvig, G. W.; Batista, V. S. *J. Inorg. Biochem.* **2006**, *100* (4), 786–800.

(18) Cady, C. W.; Shinopoulos, K. E.; Crabtree, R. H.; Brudvig, G. W. *Dalton Trans.* **2010**, *39* (16), 3985–3989.

(19) Cooper, S. R.; Calvin, M. *J. Am. Chem. Soc.* **1977**, *99* (20), 6623–6630.

(20) Kirby, J. A.; Robertson, A. S.; Smith, J. P.; Thompson, A. C.; Cooper, S. R.; Klein, M. P. *J. Am. Chem. Soc.* **1981**, *103* (18), 5529–5537.

(21) Mukhopadhyay, S.; Mandal, S. K.; Bhaduri, S.; Armstrong, W. H. *Chem. Rev.* **2004**, *104* (9), 3981–4026.

(22) Ruettinger, W. F.; Campana, C.; Dismukes, G. C. *J. Am. Chem. Soc.* **1997**, *119* (28), 6670–6671.

(23) Cady, C. W.; Crabtree, R. H.; Brudvig, G. W. *Coord. Chem. Rev.* **2008**, *252* (3-4), 444–455.

(24) Hagen, K. S.; Westmoreland, T. D.; Scott, M. J.; Armstrong, W. H. *J. Am. Chem. Soc.* **1989**, *111* (5), 1907–1909.

(25) Thorp, H. H.; Sarneski, J. E.; Brudvig, G. W.; Crabtree, R. H. *J. Am. Chem. Soc.* **1989**, *111* (26), 9249–9250.

(26) Sarneski, J. E.; Thorp, H. H.; Brudvig, G. W.; Crabtree, R. H.; Schulte, G. K. *J. Am. Chem. Soc.* **1990**, *112* (20), 7255–7260.

(27) Meyer, T. J. *Acc. Chem. Res.* **1989**, *22* (5), 163–170.

(28) Sarneski, J. E.; Didiuk, M.; Thorp, H. H.; Crabtree, R. H.; Brudvig, G. W.; Faller, J. W.; Schulte, G. K. *Inorg. Chem.* **1991**, *30* (14), 2833–2835.

(29) Nyholm, R. S.; Turco, A. *Chem. Ind. (London)* **1960**, (3), 74–75.

(30) Plaksin, P. M.; Palenik, G. J.; Stoufer, R. C.; Mathew, M. *J. Am. Chem. Soc.* **1972**, *94* (6), 2121.

(31) Thorp, H. H.; Sarneski, J. E.; Kulawiec, R. J.; Brudvig, G. W.; Crabtree, R. H.; Papaefthymiou, G. C. *Inorg. Chem.* **1991**, *30* (5), 1153–1155.

(32) Ruettinger, W. F.; Ho, D. M.; Dismukes, G. C. *Inorg. Chem.* **1999**, *38* (6), 1036+.

(33) Chen, H. Y.; Faller, J. W.; Crabtree, R. H.; Brudvig, G. W. *J. Am. Chem. Soc.* **2004**, *126* (23), 7345–7349.

(34) Brimblecombe, R.; Bond, A. M.; Dismukes, G. C.; Swiegers, G. F.; Spiccia, L. *Phys. Chem. Chem. Phys.* **2009**, *11* (30), 6441–6449.

(35) Tsai, M. K.; Rochford, J.; Polyansky, D. E.; Wada, T.; Tanaka, K.; Fujita, E.; Muckerman, J. T. *Inorg. Chem.* **2009**, *48* (10), 4372–4383.

(36) Cheng, T. Y.; Szalda, D. J.; Hanson, J. C.; Muckerman, J. T.; Bullock, R. M. *Organometallics* **2008**, *27* (15), 3785–3795.

(37) Muckerman, J. T.; Fujita, E.; Hoff, C. D.; Kubas, G. J. *J. Phys. Chem. B* **2007**, *111* (24), 6815–6821.

(38) Fujita, E.; Brunschwig, B. S.; Creutz, C.; Muckerman, J. T.; Sutin, N.; Szalda, D.; van Eldik, R. *Inorg. Chem.* **2006**, *45* (4), 1595–1603.

(39) Hou, H.; Muckerman, J. T.; Liu, P.; Rodriguez, J. A. *J. Phys. Chem. A* **2003**, *107* (44), 9344–9356.

(40) Roy, L. E.; Batista, E. R.; Hay, P. J. *Inorg. Chem.* **2008**, *47* (20), 9228–9237.

(41) Roy, L. E.; Jakubikova, E.; Guthrie, M. G.; Batista, E. R. *J. Phys. Chem. A* **2009**, *113* (24), 6745–6750.

(42) Li, J.; Fisher, C. L.; Chen, J. L.; Bashford, D.; Noodleman, L. *Inorg. Chem.* **1996**, *35* (16), 4694–4702.

(43) Baik, M. H.; Friesner, R. A. *J. Phys. Chem. A* **2002**, *106* (32), 7407–7412.

(44) Uudsemaa, M.; Tamm, T. *J. Phys. Chem. A* **2003**, *107* (46), 9997–10003.

(45) Moens, J.; Geerlings, P.; Roos, G. *Chem.—Eur. J.* **2007**, *13* (29), 8174–8184.

(46) Moens, J.; Jaque, P.; De Proft, F.; Geerlings, P. *J. Phys. Chem. A* **2008**, *112* (26), 6023–6031.

(47) Moens, J.; Roos, G.; Jaque, P.; Proft, F.; Geerlings, P. *Chem.—Eur. J.* **2007**, *13* (33), 9331–9343.

(48) Yang, X.; Baik, M. H. *J. Am. Chem. Soc.* **2006**, *128* (23), 7476–7485.

(49) Ayala, R.; Sprik, M. *J. Chem. Theory Comput.* **2006**, *2* (5), 1403–1415.

(50) Galstyan, A.; Knapp, E. W. *J. Comput. Chem.* **2009**, *30* (2), 203–211.

(51) De Groot, M. T.; Koper, M. T. M. *Phys. Chem. Chem. Phys.* **2008**, *10* (7), 1023–1031.

(52) Wang, T.; Friesner, R. A. *J. Phys. Chem. C* **2009**, *113* (6), 2553–2561.

(53) Becke, A. D. *Phys. Rev. A: At., Mol., Opt. Phys.* **1988**, *38* (6), 3098–3100.

(54) Lee, C. T.; Yang, W. T.; Parr, R. G. *Phys. Rev. B: Condens. Matter Mater. Phys.* **1988**, *37* (2), 785–789.

(55) Perdew, J. P.; Burke, K.; Ernzerhof, M. *Phys. Rev. Lett.* **1996**, *77* (18), 3865–3868.

(56) Becke, A. D. *J. Chem. Phys.* **1993**, *98* (7), 5648–5652.

(57) Becke, A. D. *J. Chem. Phys.* **1993**, *98* (2), 1372–1377.

(58) Wang, T.; Brudvig, G.; Batista, V. S. *J. Chem. Theory Comput.* **2010**, *6* (3), 755–760.

(59) Tagore, R.; Crabtree, R. H.; Brudvig, G. W. *Inorg. Chem.* **2008**, *47* (6), 1815–1823.

(60) Dismukes, G. C.; Brimblecombe, R.; Felton, G. A. N.; Pryadun, R. S.; Sheats, J. E.; Spiccia, L.; Swiegers, G. F. *Acc. Chem. Res.* **2009**, *42* (12), 1935–1943.

(61) Noodleman, L. *J. Chem. Phys.* **1981**, *74* (10), 5737–5743.

(62) Benard, M. *J. Chem. Phys.* **1979**, *71* (6), 2546–2556.

(63) Dunning, T. H. *J. Chem. Phys.* **1989**, *90* (2), 1007–1023.

(64) Kendall, R. A.; Dunning, T. H.; Harrison, R. J. *J. Chem. Phys.* **1992**, *96* (9), 6796–6806.

(65) Woon, D. E.; Dunning, T. H. *J. Chem. Phys.* **1993**, *98* (2), 1358–1371.

(66) Reiss, H.; Heller, A. *J. Phys. Chem.* **1985**, *89* (20), 4207–4213.

(67) Rashin, A. A.; Honig, B. *J. Phys. Chem.* **1985**, *89* (26), 5588–5593.

(68) Marten, B.; Kim, K.; Cortis, C.; Friesner, R. A.; Murphy, R. B.; Ringnalda, M. N.; Sitkoff, D.; Honig, B. *J. Phys. Chem.* **1996**, *100* (28), 11775–11788.

(69) Jang, Y. H.; Sowers, L. C.; Cagin, T.; Goddard, W. A. *J. Phys. Chem. A* **2001**, *105* (1), 274–280.

(70) Lim, C.; Bashford, D.; Karplus, M. *J. Phys. Chem.* **1991**, *95* (14), 5610–5620.

(71) Morrison, M. M.; Sawyer, D. T. *J. Am. Chem. Soc.* **1977**, *99* (1), 257–258.

CT1002658